

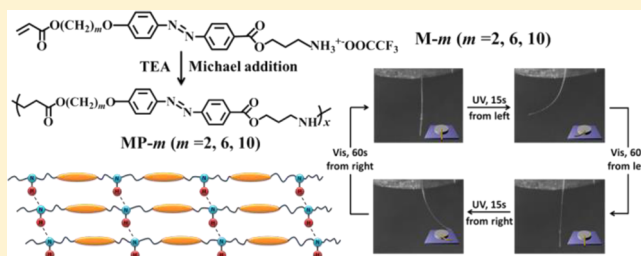
# Synthesis of Reactive Azobenzene Main-Chain Liquid Crystalline Polymers via Michael Addition Polymerization and Photomechanical Effects of Their Supramolecular Hydrogen-Bonded Fibers

Liangjing Fang, Hongtao Zhang, Zidong Li, Ying Zhang, Yuying Zhang, and Huiqi Zhang\*

Key Laboratory of Functional Polymer Materials, Ministry of Education, Synergetic Innovation Center of Chemical Science and Engineering (Tianjin), and Department of Chemistry, Nankai University, Tianjin 300071, People's Republic of China

## Supporting Information

**ABSTRACT:** A new and efficient strategy for obtaining a series of reactive azobenzene (azo)-containing main-chain liquid crystalline polymers (LCPs) is described, which involves the first design and synthesis of acrylate-type azo monomers with different length of flexible spacers and an amino end-group (in its trifluoroacetate salt form) and their subsequent Michael addition polymerization under mild reaction conditions. The resulting polymers showed rather high thermal stability, relatively low glass transition temperatures, a broad temperature range of smectic C liquid crystalline phase, and reversible photoresponsive behavior. The presence of secondary amino groups in the backbones of these azo main-chain LCPs not only made them highly reactive precursors for various new functional linear and cross-linked azo LCPs but also led to the formation of hydrogen-bonding interactions among their polymer chains. Supramolecular hydrogen-bonding cross-linked LCP fibers were directly fabricated by using the simple melt spinning method, which proved to have a high order of mesogen along the fiber axis and exhibit good mechanical properties, fast and reversible photoinduced bending and unbending behaviors, and large photoinduced stress (240 kPa) at close to ambient temperature as well as excellent photodeformation fatigue resistance.



## INTRODUCTION

Azobenzene (azo)-containing liquid crystalline polymers (LCPs) have drawn considerable attention in recent years because of their combined intriguing properties of anisotropic liquid crystals, photoresponsive materials, and flexible polymers.<sup>1–17</sup> The liquid crystalline properties of the azo polymers are related to the rod-like *trans*-azo mesogens, and their photoresponsive properties stem from the photoinduced fast and reversible isomerization between the *trans* and *cis* isomers of the azo groups upon exposure to UV or visible light, which triggers significant changes in their physicochemical properties and can lead to photoinduced reorientation of azo groups in the polymers. Many potential applications have been proposed for these polymers, such as optical data storage, liquid crystal displays, molecular switches, nonlinear optical devices, surface relief gratings, and photomechanical systems.

So far, a great number of azo LCPs with various structures have been developed for different purposes, such as comb-shaped LCPs with azo mesogens in the side chains,<sup>1–4,6,13</sup> LCPs with azo units in the main chains,<sup>1,12</sup> and cross-linked azo LCPs.<sup>4,5,7–12,14–17</sup> In addition, azo LCPs can also be classified into nonreactive and reactive ones, depending on whether they contain reactive groups or not. Among them, the reactive azo LCPs are particularly interesting because they could offer many new possibilities for generating advanced photoresponsive materials by their transformation into cross-linked LCP networks through the cross-linking or by their further

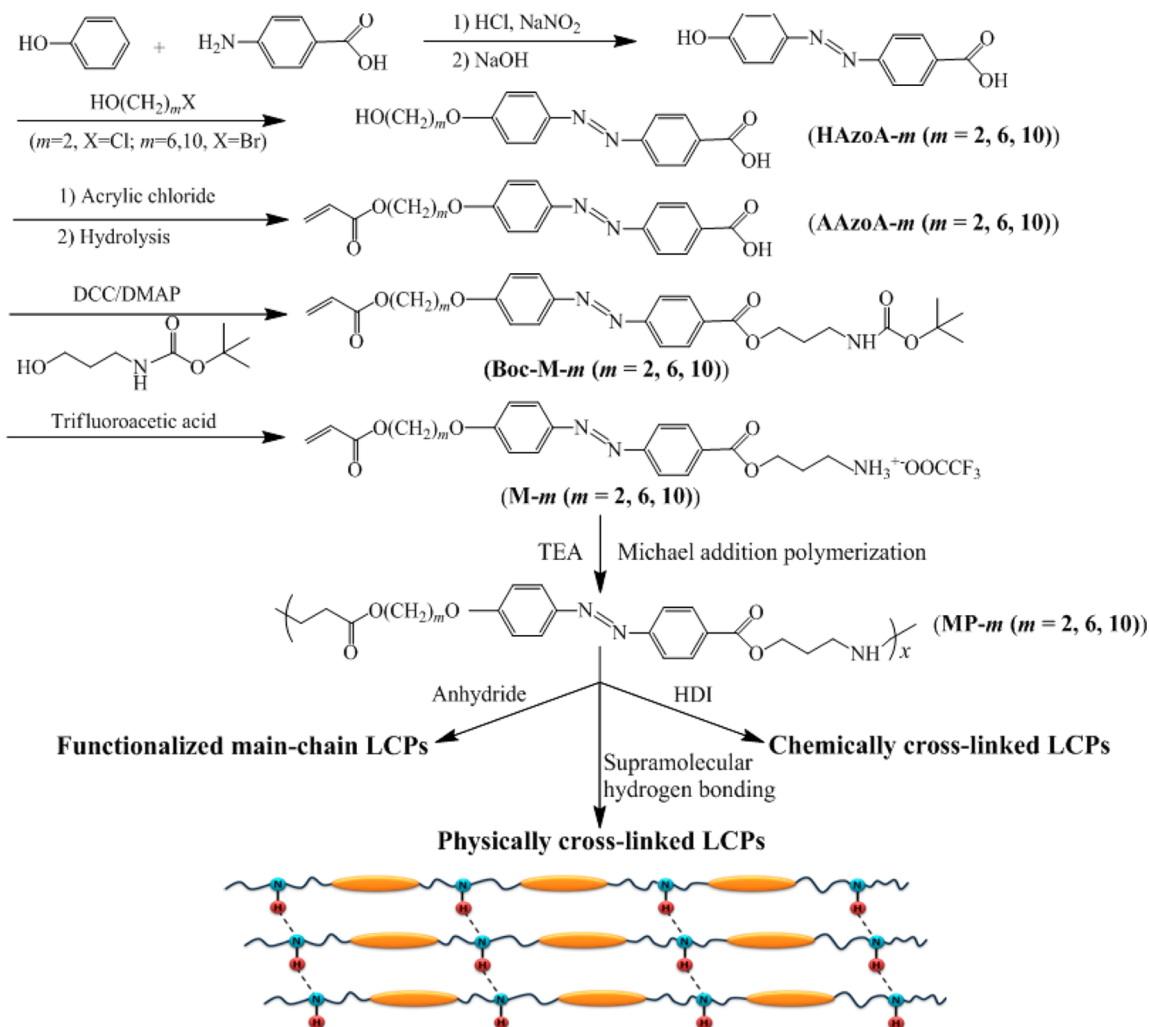
modification with other functional species, which makes them highly promising functional materials for such applications as the improvement of the thermal stability of the photoinduced surface relief grating,<sup>18–20</sup> preparation of photoresponsive liquid crystalline elastomers (LCEs) for photomechanical devices,<sup>8,9,12,21–23</sup> and so forth.

In general, the reactive azo LCPs can be divided into side-chain and main-chain types according to the location of the azo groups in the polymers. Since the reactive azo side-chain LCPs can be easily prepared either by the copolymerization of a monovinyl azo monomer without a reactive group and another monovinyl monomer with a reactive group<sup>18,22,24</sup> or by the direct polymerization of a monovinyl azo monomer with a reactive group,<sup>23,25,26</sup> such functional side-chain azo LCPs have been prepared and used in different areas in most cases. In sharp contrast, the reactive azo main-chain LCPs have been rarely reported up to now,<sup>27</sup> although they have some distinct advantages over the side-chain ones such as their better thermal stability<sup>28</sup> and much stronger chain anisotropy,<sup>12</sup> which is probably due to the availability of rather limited synthetic methods.<sup>28</sup> As far as we know, only Acierno et al. reported the synthesis of a series of reactive main-chain segmented azo LCPs with pendent vinyl groups via solution polycondensation

Received: August 7, 2013

Revised: August 31, 2013

**Scheme 1. Synthetic Route and Chemical Structures of the Acrylate-Type Azo Monomers with an Amino End-Group in Its Trifluoroacetate Salt Form ( $M-m$  ( $m = 2, 6, 10$ )) and Their Main-Chain LCPs ( $MP-m$  ( $m = 2, 6, 10$ )) Prepared via Michael Addition Polymerization as Well as the Chemical Reactivity and Supramolecular Hydrogen Bonding Interaction of These Main-Chain LCPs (TEA: Triethylamine; HDI: 1,6-Hexamethylene Diisocyanate)**



approach and studies on their photoresponsive properties both in the solutions and in thin films.<sup>27</sup> In addition, several main-chain azo polymers bearing reactive groups have also been prepared for different purposes, but they did not show liquid crystalline properties.<sup>29–33</sup> On the basis of the above statements, it can be concluded that despite the promising future of reactive azo main-chain LCPs in many applications, their synthesis still remains a challenge. Therefore, the development of new azo-containing main-chain LCPs bearing reactive substituents (particularly those with high reactivity under mild conditions) is of significant importance.

Herein, we report for the first time an efficient strategy for preparing a series of azo main-chain LCPs with reactive secondary amino groups in the polymer backbones (i.e.,  $MP-m$  ( $m = 2, 6, 10$ ), Scheme 1) by the rational design and synthesis of acrylate-type azo monomers with different length of flexible spacers and an amino end-group in its trifluoroacetate salt form ( $M-m$  ( $m = 2, 6, 10$ )) and their subsequent Michael addition polymerization in the presence of triethylamine (TEA) under mild reaction conditions. Note that although Michael addition between acrylates and amines has found widespread applications in the macromolecular design due to its mild

reaction conditions, high functional group tolerance, and high conversions,<sup>34</sup> the preparation of LCPs with azo units in their main chains by Michael addition reaction has never been reported. The chemical structures, thermal and phase transition properties, and photoresponsivity of the resulting main-chain azo polymers were characterized in detail. In addition, the high chemical reactivity of these main-chain azo polymers and the photoinduced bending behaviors of the supramolecular hydrogen-bonded LCP fibers made from them by the simple melt spinning method were also demonstrated. *To our knowledge, the findings we report here represent the first successful example of the supramolecular photomechanical system based on the main-chain LCPs with azo mesogens in their backbones that can show good mechanical properties, fast and reversible photoinduced bending and unbending behaviors and large photoinduced stress at close to ambient temperature, and excellent photodeformation fatigue resistance.*

## EXPERIMENTAL SECTION

**Materials.** Tetrahydrofuran (THF, Tianjin Jiangtian Chemicals, China, 99%) was refluxed over sodium and then distilled. Dichloromethane (CH<sub>2</sub>Cl<sub>2</sub>, Tianjin Jiangtian Chemicals, 99%) and chloroform

(CHCl<sub>3</sub>, Tianjin Jiangtian Chemicals, 99%) were refluxed over calcium hydride and then distilled. *N,N*-Dimethylformamide (DMF, Tianjin Jiangtian Chemicals, 99.5%) was dried with anhydrous magnesium sulfate and then distilled under vacuum. Triethylamine (TEA, Tianjin Jiangtian Chemicals, 99%) was dried with anhydrous sodium sulfate and then distilled. Thionyl chloride (Tianjin Jiangtian Chemicals, 99.5%) was purified by distillation just prior to use. Methacryloyl chloride was prepared by the reaction between methacrylic acid (Tianjin Jiangtian Chemicals, 99%) and thionyl chloride. Methacrylic anhydride was prepared by reacting methacrylic acid with methacryloyl chloride in the presence of an aqueous solution of sodium hydroxide. Acrylic chloride was prepared by the reaction between acrylic acid (Tianjin Damao Chemical Reagent Factory, China, 99.5%) and benzoyl chloride (Tianjin Jiangtian Chemicals, 98%). 4-((4-Hydroxy)phenylazo)benzoic acid, 4-((4-*ω*-hydroxyalkoxy)phenylazo)benzoic acid (HAzoA-*m* (*m* = 2, 6, 10)), and 4-((4-*ω*-acryloyloxyalkoxy)phenylazo)benzoic acid (AAzoA-*m* (*m* = 2, 6, 10)) were synthesized according to our previously reported procedure (Scheme 1).<sup>35,36</sup> 3-(*tert*-Butoxycarbonylamino)-1-propanol was prepared following a literature method.<sup>37</sup> 4-(Dimethylamino)pyridine (DMAP, Merck, analytical grade (AR)), *N,N'*-dicyclohexylcarbodiimide (DCC, Tianjin Jiangtian Chemicals, AR), and all the other chemicals were commercially available and used without further purification.

**3-(*tert*-Butoxycarbonylamino)-1-Propyl 4-((4-*ω*-Acryloyloxyethoxy)phenylazo)benzoate (Boc-M-2).** AAzoA-2 (3.40 g, 10 mmol), 3-(*tert*-butoxycarbonylamino)-1-propanol (3.50 g, 20 mmol), and DMAP (0.244 g, 2 mmol) were dissolved in dried THF (150 mL), and the solution was cooled to 0 °C. To this mixture was added dropwise a solution of DCC (1.94 g, 10 mmol) in dried THF (50 mL) with stirring. After being stirred at ambient temperature for 24 h, the reaction mixture was filtered and the filtrate was poured into a large amount of water (400 mL). The resulting precipitate was collected and then purified with silica gel column chromatography by using a mixture of ethyl acetate and CH<sub>2</sub>Cl<sub>2</sub> (1/12 v/v) as the eluent to provide an orange product (yield: 70%). Melting point (mp) 104–106 °C (determined by polarizing optical microscope (POM) at a heating rate of 10 °C/min). UV-vis (DMF): λ<sub>max</sub>/nm (ε/L mol<sup>-1</sup> cm<sup>-1</sup>) = 362 (26 640), around 450 (not available due to the overlap of the absorption bands). <sup>1</sup>H NMR (400 MHz, DMSO-*d*<sub>6</sub>): δ (ppm) = 8.24–8.13 (d, 2H, Ar-H), 8.02–7.90 (m, 4H, Ar-H), 7.27–7.17 (d, 2H, Ar-H), 6.98–6.87 (br, 1H, -NH), 6.42–6.33 (dd, 1H, CH=C-COO-), 6.29–6.18 (dd, 1H, C=CH-COO-), 6.05–5.95 (dd, 1H, CH=C-COO-), 4.57–4.47 (t, 2H, Ar-COOCH<sub>2</sub>-), 4.44–4.38 (t, 2H, C=C-COOCH<sub>2</sub>-), 4.35–4.27 (t, 2H, Ar-OCH<sub>2</sub>-), 3.18–3.04 (q, 2H, -CH<sub>2</sub>N-), 1.92–1.81 (m, 2H, -CH<sub>2</sub>CN-), 1.37 (s, 9H, -CH<sub>3</sub>).

**3-(*tert*-Butoxycarbonylamino)-1-Propyl 4-((4-*ω*-Acryloyloxyhexyloxy)phenylazo)benzoate (Boc-M-6).** Prepared as for Boc-M-2 (yield: 65%); mp 96–98 °C (determined by POM at a heating rate of 10 °C/min). UV-vis (DMF): λ<sub>max</sub>/nm (ε/L mol<sup>-1</sup> cm<sup>-1</sup>) = 363 (27 200), around 450 (not available due to the overlap of the absorption bands). <sup>1</sup>H NMR (400 MHz, DMSO-*d*<sub>6</sub>): δ (ppm) = 8.22–8.12 (d, 2H, Ar-H), 8.03–7.91 (m, 4H, Ar-H), 7.20–7.12 (d, 2H, Ar-H), 7.02–6.93 (br, 1H, -NH), 6.38–6.29 (dd, 1H, CH=C-COO-), 6.24–6.13 (dd, 1H, C=CH-COO-), 5.98–5.91 (dd, 1H, CH=C-COO-), 4.37–4.27 (t, 2H, Ar-COOCH<sub>2</sub>-), 4.16–4.06 (m, 4H, C=C-COOCH<sub>2</sub>- and Ar-OCH<sub>2</sub>-), 3.16–3.06 (q, 2H, -CH<sub>2</sub>N-), 1.93–1.29 (m, 10H, -(CH<sub>2</sub>)<sub>4</sub>- and -CH<sub>2</sub>CN-), 1.38 (s, 9H, -CH<sub>3</sub>).

**3-(*tert*-Butoxycarbonylamino)-1-Propyl 4-((4-*ω*-Acryloyloxydecyloxy)phenylazo)benzoate (Boc-M-10).** Prepared as for Boc-M-2 (yield: 67%); mp 92–94 °C (determined by POM at a heating rate of 10 °C/min). UV-vis (DMF): λ<sub>max</sub>/nm (ε/L mol<sup>-1</sup> cm<sup>-1</sup>) = 363 (26 840), around 450 (not available due to the overlap of the absorption bands). <sup>1</sup>H NMR (400 MHz, DMSO-*d*<sub>6</sub>): δ (ppm) = 8.28–8.14 (d, 2H, Ar-H), 8.08–7.92 (m, 4H, Ar-H), 7.26–7.14 (d, 2H, Ar-H), 7.04–6.93 (br, 1H, -NH), 6.42–6.31 (dd, 1H, CH=C-COO-), 6.25–6.13 (dd, 1H, C=CH-COO-), 6.01–5.91 (dd, 1H, CH=C-COO-), 4.39–4.28 (t, 2H, Ar-COOCH<sub>2</sub>-), 4.19–4.06 (m, 4H, C=C-COOCH<sub>2</sub>- and Ar-OCH<sub>2</sub>-), 3.19–3.08

(q, 2H, -CH<sub>2</sub>N-), 1.94–1.19 (m, 18H, -(CH<sub>2</sub>)<sub>8</sub>- and -CH<sub>2</sub>CN-), 1.39 (s, 9H, -CH<sub>3</sub>).

**Trifluoroacetate Salt of 3-Amino-1-Propyl 4-((4-*ω*-Acryloyloxyethoxy)phenylazo)benzoate (M-2).** Trifluoroacetic acid (27 mL, 0.36 mol) was added dropwise into a solution of Boc-M-2 (1.78 g, 3.6 mmol) in dried CH<sub>2</sub>Cl<sub>2</sub> (27 mL) in an ice bath. The reaction mixture was then stirred at ambient temperature for 5 h, which was subsequently poured into a large amount of ether (250 mL). The precipitate was filtered, washed with ether several times, and then dried under vacuum at 40 °C for 24 h to obtain the orange-yellow product (yield: 93%); mp 132–134 °C (determined by POM at a heating rate of 10 °C/min). UV-vis (DMF): λ<sub>max</sub>/nm (ε/L mol<sup>-1</sup> cm<sup>-1</sup>) = 360 (23 680), around 450 (not available due to the overlap of the absorption bands). <sup>1</sup>H NMR (400 MHz, DMSO-*d*<sub>6</sub>): δ (ppm) = 8.24–8.14 (d, 2H, Ar-H), 8.02–7.94 (m, 4H, Ar-H), 7.88–7.72 (br, 3H, -NH<sub>3</sub>), 7.29–7.17 (d, 2H, Ar-H), 6.43–6.34 (dd, 1H, CH=C-COO-), 6.30–6.19 (dd, 1H, C=CH-COO-), 6.02–5.95 (dd, 1H, CH=C-COO-), 4.54–4.47 (t, 2H, Ar-COOCH<sub>2</sub>-), 4.43–4.34 (m, 4H, C=C-COOCH<sub>2</sub>- and Ar-OCH<sub>2</sub>-), 3.06–2.97 (t, 2H, -CH<sub>2</sub>N-), 2.11–1.98 (m, 2H, -CH<sub>2</sub>CN-).

**Trifluoroacetate Salt of 3-Amino-1-Propyl 4-((4-*ω*-Acryloyloxyhexyloxy)phenylazo)benzoate (M-6).** Prepared as for M-2 (yield: 95%); mp 131–133 °C (determined by POM at a heating rate of 10 °C/min). UV-vis (DMF): λ<sub>max</sub>/nm (ε/L mol<sup>-1</sup> cm<sup>-1</sup>) = 361 (23 900), around 450 (not available due to the overlap of the absorption bands). <sup>1</sup>H NMR (400 MHz, DMSO-*d*<sub>6</sub>): δ (ppm) = 8.29–8.15 (d, 2H, Ar-H), 8.02–7.91 (m, 4H, Ar-H), 7.89–7.78 (br, 3H, -NH<sub>3</sub>), 7.21–7.13 (d, 2H, Ar-H), 6.37–6.29 (dd, 1H, CH=C-COO-), 6.21–6.13 (dd, 1H, C=CH-COO-), 5.95–5.91 (dd, 1H, CH=C-COO-), 4.43–4.37 (t, 2H, Ar-COOCH<sub>2</sub>-), 4.17–4.07 (m, 4H, C=C-COOCH<sub>2</sub>- and Ar-OCH<sub>2</sub>-), 3.07–2.98 (t, 2H, -CH<sub>2</sub>N-), 2.10–1.35 (m, 10H, -(CH<sub>2</sub>)<sub>4</sub>- and -CH<sub>2</sub>CN-).

**Trifluoroacetate Salt of 3-Amino-1-Propyl 4-((4-*ω*-Acryloyloxydecyloxy)phenylazo)benzoate (M-10).** Prepared as for M-2 (yield: 96%); mp 129–131 °C (determined by POM at a heating rate of 10 °C/min). UV-vis (DMF): λ<sub>max</sub>/nm (ε/L mol<sup>-1</sup> cm<sup>-1</sup>) = 361 (24 120), around 450 (not available due to the overlap of the absorption bands). <sup>1</sup>H NMR (400 MHz, DMSO-*d*<sub>6</sub>): δ (ppm) = 8.25–8.15 (d, 2H, Ar-H), 8.04–7.91 (m, 4H, Ar-H), 7.89–7.72 (br, 3H, -NH<sub>3</sub>), 7.24–7.13 (d, 2H, Ar-H), 6.36–6.28 (dd, 1H, CH=C-COO-), 6.22–6.13 (dd, 1H, C=CH-COO-), 5.97–5.91 (dd, 1H, CH=C-COO-), 4.43–4.35 (t, 2H, Ar-COOCH<sub>2</sub>-), 4.15–4.05 (m, 4H, C=C-COOCH<sub>2</sub>- and Ar-OCH<sub>2</sub>-), 3.07–2.97 (t, 2H, -CH<sub>2</sub>N-), 2.10–1.22 (m, 18H, -(CH<sub>2</sub>)<sub>8</sub>- and -CH<sub>2</sub>CN-).

**Synthesis of the Main-Chain Azo Polymers (MP-*m* (*m* = 2, 6, 10)) via Michael Addition Polymerization.** The typical Michael addition polymerization of M-6 is presented as follows: M-6 (1.134 g, 2 mmol), triethylamine (TEA, 0.58 mL, 4 mmol), and a mixture of freshly distilled methanol and DMF (1/1 v/v, 80 mL) were added into a one-neck round-bottom flask (250 mL) successively, and a clear solution was obtained after the ultrasonic treatment. The reaction mixture was bubbled with argon for 20 min, sealed, and then immersed into a thermostated oil bath at 40 °C in the dark. After a certain time of polymerization with stirring (note that the precipitation of the resulting polymers was observed during the polymerization process), the reaction mixture was cooled to room temperature and then poured into methanol (200 mL). The precipitate was filtered, and the obtained solid was washed thoroughly with warm methanol until no monomer was detected with thin layer chromatography. Finally, the product was dried at 40 °C under vacuum for 24 h to provide the orange-yellow main-chain azo polymer MP-6. The yield of MP-6 was 34, 40, 54, 56, and 58% for a polymerization time of 3, 6, 12, 24, and 48 h, respectively (Figure S1 in the Supporting Information).

Michael addition polymerizations of M-2 and M-10 were performed similarly as for M-6 except that the polymerization time was fixed at 24 h, leading to their corresponding orange-yellow main-chain azo polymers MP-2 and MP-10 in a yield of 46% and 64%, respectively.

**Cross-Linking of the Main-Chain Azo Polymer MP-6.** The synthesis of the cross-linked main-chain azo polymers CL-MP-6 (*f* = 2, 4) (CL-MP-6 refers to the cross-linked MP-6 and *f* represents the

molar ratio of the repeat unit (or reactive secondary amino group) in the main-chain azo polymer to 1,6-hexamethylene diisocyanate (HDI)) by cross-linking MP-6 with HDI was performed as follows: MP-6 (22.7 mg, 0.05 mmol of repeat unit in MP-6) was dissolved in dried chloroform (1 mL). After the solution was bubbled with argon in an ice bath for 5 min, HDI (0.025 mmol) was added. The reaction mixture was further bubbled with argon for 10 min in an ice bath, and the flask was then sealed and immersed into a thermostated oil bath at 60 °C. Finally, the cross-linked product was washed thoroughly with warm methanol and then dried at 40 °C under vacuum for 24 h to provide orange-yellow CL-MP-6-2 (yield: 87%).

CL-MP-6-4 was prepared similarly as for CL-MP-6-2, but a lower amount of HDI (0.0125 mmol) was added into the reaction system. The yield of CL-MP-6-4 was 85%.

**Polymer Analogous Reactions of MP-*m* (*m* = 2, 6, 10) with Anhydrides.** A typical procedure for the polymer analogous reaction of MP-6 with an anhydride is presented as follows (Scheme S1 in the Supporting Information): MP-6 (22.7 mg, 0.05 mmol of repeat unit in MP-6) was dissolved in dried chloroform (2 mL). To this solution was added acetic anhydride (0.2 mL, 2 mmol). After being stirred at ambient temperature for 5 h, the reaction mixture was poured into ether (20 mL). The precipitate was collected through centrifugation, washed with ether, and then dried at 40 °C under vacuum for 24 h to provide the orange-yellow acetic anhydride-modified main-chain azo polymer A-MP-6 (yield: 96%).

The polymer analogous reactions of MP-6 with Boc anhydride (or namely di-*tert*-butyl dicarbonate) and methacrylic anhydride were performed similarly following the above procedure, leading to the corresponding orange-yellow anhydride-modified main-chain polymers B-MP-6 and M-MP-6 in a yield of 91% and 93%, respectively.

Acetic anhydride-modified main-chain azo polymers MP-2 and MP-10 (i.e., A-MP-2 and A-MP-10) were prepared similarly as for A-MP-6, and the yields of A-MP-2 and A-MP-10 were 96% and 95%, respectively.

**Fabrication of MP-*m* (*m* = 2, 6, 10) Fibers.** The main-chain azo polymer fibers were prepared by using the simple melt spinning method as reported previously,<sup>23,38</sup> but in the absence of any chemical cross-linker. A typical procedure for the fabrication of MP-6 fiber is presented as follows: 5 mg of MP-6 was heated to 200 °C on a glass slide placed on a hot stage (IKA, C-MAG HP 7), which was kept at that temperature for 2 min (the sample was in an isotropic state). The temperature was then gradually lowered to 130 °C where the sample was in a liquid crystalline state. The MP-6 fiber was then drawn by dipping the tip of a metallic tweezer into the melt sample and pulling it quickly.

The MP-2 and MP-10 fibers were fabricated similarly as for the MP-6 fiber, except that the spinning temperature was changed from 130 °C for MP-6 to 115 and 120 °C for MP-2 and MP-10, respectively.

**Characterization.** <sup>1</sup>H NMR spectra were recorded on a Varian Unity plus-400 spectrometer (400 MHz). The molecular weights and molar mass dispersities (*D*) of the acetic anhydride-modified main-chain azo polymers (i.e., A-MP-*m* (*m* = 2, 6, 10)) were determined with a gel permeation chromatograph (GPC) equipped with an Agilent 1200 series manual injector, an Agilent 1200 HPLC pump, an Agilent 1200 refractive index detector, and two Waters Styragel HT columns (HT 4 and HT 3) with 5K-600 K and 500–30K molecular ranges. Chloroform was used as the eluent at a flow rate of 1.0 mL min<sup>-1</sup>. The calibration curve was obtained by using polystyrene (PS) standards. Thermogravimetric analyses (TGA) were performed on a Netzsch TG 209 instrument in a nitrogen atmosphere at a heating rate of 10 °C min<sup>-1</sup>. Differential scanning calorimetry (DSC, Netzsch 200 F3) was utilized to study the phase transitions of the azo polymers at a heating/cooling rate of 10 °C min<sup>-1</sup> under nitrogen. The temperature and heat flow scale were calibrated with standard materials including indium (70–190 °C), tin (150–270 °C), zinc (350–450 °C), bismuth (190–310 °C), and mercury (–100–0 °C) in different temperature ranges. The glass transition temperatures (*T*<sub>g</sub>) of the azo polymers were determined as the midpoints of the step changes of the heat capacities, while the phase transition temperatures were measured from the maximum/minimum of the endothermic/exothermic peaks.

The melting points of the azo monomers, the liquid crystalline textures of the azo polymers, and the alignment states of the polymer fibers were observed by using an Olympus BX51 polarizing optical microscope (POM, with crossed polarizer and analyzer) equipped with a Linksys 32 THMSE600 hot stage and a digital camera (Micropublisher 5.0 RTV). Small-angle X-ray scattering (SAXS) measurements were carried out on a Bruker NanoSTAR SAXS system using Cu K $\alpha$  ( $\lambda$  = 1.542 Å) as the radiation source. The working voltage and current are 40 kV and 35 mA, respectively. The distance between the sample and the detector is 27.15 cm. A temperature control unit in conjunction with the instrument was utilized to study the structure evaluations of the liquid crystalline mesophases by heating the samples to the desired temperatures. A Bio-Rad FTS6000 FT-IR spectrometer equipped with an UMA-500 microscope, an MCT detector (cooled with liquid nitrogen), and a Linkam FTIR600 hot stage and temperature control system was utilized to carry out the variable temperature FT-IR measurements. The studied polymer sample was sandwiched between two KBr slides, and its temperature was changed at a rate of 10 °C min<sup>-1</sup>. Sixteen scans were conducted for each spectrum at the selected temperatures in the wavenumber range of 700–4000 cm<sup>-1</sup> with a resolution of 8 cm<sup>-1</sup>. An UV-vis scanning spectrophotometer (TU1900, Beijing Purkinje General Instrument Co., Ltd.) was utilized to obtain the UV-vis spectra of the studied azo monomer and polymer solutions at 25 °C. The photochemical isomerization of the polymer solution was investigated by irradiating it first with a 365 nm UV lamp (12 W) until the photostationary state was reached and then with a 450 nm visible light lamp (18 W, wavelength range 400–550 nm,  $\lambda_{\text{max}}$  = 450 nm; a filter was put between the samples and the lamp during the study in order to block the light with wavelength  $\lambda$  < 430 nm). The photoinduced bending and unbending behaviors of the MP-*m* (*m* = 2, 6, 10) fibers were investigated as follows: Part of a polymer fiber was first pasted onto an aluminum block, which was heated to a certain temperature with a hot stage under the control of a thermocouple (IKA C-MAG HP 7). Irradiation of the polymer fiber with 365 nm UV light and visible light ( $\lambda$  > 430 nm) was performed using a high-pressure mercury lamp (USHIO SP-7) through glass filters. The photographs of the bending and unbending behaviors of the polymer fiber were taken by using a CCD camera (KBier-1202). The UV-induced bending and thermally induced unbending behaviors of the MP-6 fiber were investigated similarly. Thermomechanical analysis (TMA) was performed in a stretch mode under an external tension at a constant temperature by using a dynamic mechanical analyzer (DMA) (TA Instruments, DMA-Q800) to study the mechanical properties (at 28 °C) and photoinduced stress (at 35 °C) of the azo main-chain LCP fibers.

## RESULTS AND DISCUSSION

**Synthesis and Characterization of the Reactive Azo Main-Chain LCPs.** It has been well demonstrated that the Michael addition between acrylates and amines is highly versatile in the macromolecular design due to its mild reaction conditions, high functional group tolerance, and high conversions.<sup>34</sup> Therefore, it can be expected that Michael addition polymerization of the acrylate-type azo monomers with an amino end-group should take place easily under suitable reaction conditions, leading to the main-chain azo polymers (Scheme 1). To confirm our hypothesis, a series of acrylate-type azo monomers with different length of flexible spacers and an amino end-group in its trifluoroacetate salt form (i.e., trifluoroacetate salt of 3-amino-1-propyl 4-((4-*o*-acryloyloxyalkoxy))phenylazo)benzoate, M-*m* (*m* = 2, 6, 10)) were first designed and synthesized according to the synthetic route illustrated in Scheme 1. 4-((4-Hydroxy)phenylazo)benzoic acid, 4-((4-*o*-hydroxyalkoxy)phenylazo)benzoic acid (HAzoA-*m*, *m* = 2, 6, 10), and 4-((4-*o*-acryloyloxyalkoxy)phenylazo)benzoic acid (AAzoA-*m*, *m* =

2, 6, 10) were prepared according to our previously reported procedure.<sup>35,36</sup> 3-(*tert*-Butoxycarbonylamino)-1-propyl 4-((4-(*ω*-acryloyloxyalkoxy))phenylazo)benzoate (Boc-M-*m*, *m* = 2, 6, 10) was readily prepared in quite good yields (65–70%) through the coupling reaction between AAzoA-*m* (*m* = 2, 6, 10) and 3-(*tert*-butoxycarbonylamino)-1-propanol in the presence of DMAP and DCC. Boc-M-*m* (*m* = 2, 6, 10) were then reacted with trifluoroacetic acid to provide the deprotected acrylate azo monomers with an amino group in its trifluoroacetate salt form (M-*m* (*m* = 2, 6, 10)) in almost quantitative yields. The purity of Boc-M-*m* and M-*m* (*m* = 2, 6, 10) was satisfactory, as verified with both thin layer chromatography and the <sup>1</sup>H NMR technique (Figure 1a,b).

The Michael addition polymerization of M-6 was first carried out by stirring it with TEA in a mixture of freshly distilled methanol and DMF (1/1 v/v) under argon at 40 °C for different times. A series of orange-yellow azo polymers (MP-6) were readily obtained by pouring the reaction mixtures into methanol and thoroughly washing the resulting precipitates with warm methanol until no monomer could be detected by thin layer chromatography and <sup>1</sup>H NMR technique. The yields of the azo polymer MP-6 proved to be dependent on the polymerization time, and they increased largely in the first 12 h and then almost leveled off at a polymerization time of 24 h (yield = 56%) (Figure S1). Therefore, the Michael addition polymerizations of M-2 and M-10 were also performed similarly as for M-6 for a reaction time of 24 h, leading to their corresponding orange-yellow azo polymers MP-2 and MP-10 in a yield of 46% and 64%, respectively. All the obtained azo polymers proved to be soluble in chloroform (instead of THF). In this context, it is worth mentioning that although methanol is a nonsolvent for our azo polymers, its combined use with DMF as the solvent for the Michael addition polymerization proved to lead to considerably enhanced polymerization rates and azo polymers with relatively high molecular weights.

The <sup>1</sup>H NMR spectra of one representative azo polymer MP-6 and its acetamide A-MP-6 (Scheme S1) are shown in Figure 1c,d. A detailed comparison of the proton signals from the methylene groups connected with the nitrogen atom in MP-6 and A-MP-6 revealed the presence of a secondary amino group in the repeat unit of MP-6 instead of a tertiary one because the acetamidation of MP-6 led to the significant shift of these methylene proton signals (i.e., peaks a and m). This result demonstrates that the azo polymers prepared by Michael addition polymerization are indeed main-chain linear polymers instead of hyperbranched ones. In addition, the chemical shifts and peak integrations of all the protons in the polymer are in excellent agreement with its expected structure.

The molecular weights and molar mass dispersities ( $\bar{D}$ ) of MP-*m* (*m* = 2, 6, 10) were characterized by using GPC with chloroform as the eluent. However, no GPC signal was observed for these polymers, probably due to the existence of strong interaction between the secondary amino groups of the polymers and GPC columns. This hypothesis was verified by the fact that the molecular weights and  $\bar{D}$  values of the azo polymers were readily obtained by GPC after they were allowed to react with acetic anhydride to protect their secondary amino groups. The number-average molecular weights of the resulting polymers (i.e., A-MP-*m* (*m* = 2, 6, 10)) determined by GPC (i.e.,  $M_{n,GPC}$ ) proved to range from 6800 to 7230, and their  $\bar{D}$  values were around 1.5 (Table 1).

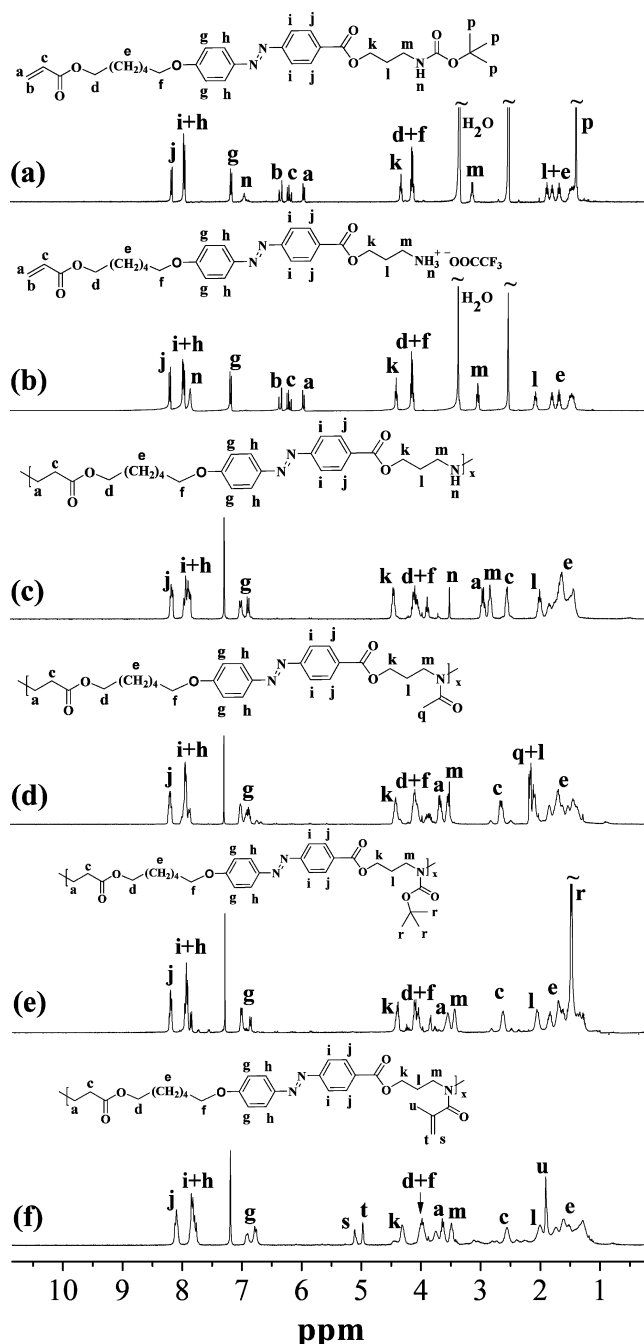


**Figure 1.** <sup>1</sup>H NMR spectra of Boc-M-6 (a) and M-6 (b) in DMSO-*d*<sub>6</sub> and those of MP-6 (c), A-MP-6 (d), B-MP-6 (e), and M-MP-6 (f) in CDCl<sub>3</sub>.

The thermal and phase transition behaviors of the main-chain azo polymers MP-*m* (*m* = 2, 6, 10) were then studied by using TGA, DSC, POM, and SAXS. The temperatures at 5% weight loss of the polymers determined by TGA under nitrogen were found to be  $\geq 271$  °C, demonstrating their rather good thermal stability (Table 1). The DSC study showed that all the main-chain azo polymers exhibited one glass transition step and one phase transition peak during both the second heating and the first cooling scans (Figure 2). A glass transition temperature ( $T_g$ ) of 50, 30, and 43 °C was observed in the DSC second heating scan for MP-2, MP-6, and MP-10, respectively (Table 1). The POM observation revealed that there existed enantiotropic schlieren liquid crystalline textures for all the

**Table 1. Characterization and Thermal Transition Data of the Azo Main-Chain LCPs**

sample	yield <sup>a</sup> (%)	$M_{n,GPC}$ <sup>b</sup>	$D$ <sup>b</sup>	thermal transition <sup>c</sup> $T$ (°C)	$\Delta H_{it}^f$ (kJ/mol)	$T_g^g$ (°C)
MP-2	46	6800	1.46	G 50 S <sub>C</sub> 139 I <sup>d</sup>	3.0	271
				I 133 S <sub>C</sub> 46 G <sup>e</sup>	-3.3	
MP-6	56	6960	1.52	G 30 S <sub>C</sub> 159 I <sup>d</sup>	11.2	277
				I 148 S <sub>C</sub> 27 G <sup>e</sup>	-10.1	
MP-10	64	7230	1.51	G 43 S <sub>C</sub> 142 I <sup>d</sup>	12.5	284
				I 129 S <sub>C</sub> 44 G <sup>e</sup>	-11.4	

<sup>a</sup>All the polymers were obtained at a polymerization time of 24 h.

<sup>b</sup>The number-average molecular weights ( $M_{n,GPC}$ ) and molar mass dispersities ( $D$ ) of the polymers were determined by GPC with chloroform as the eluent after their modification with acetic anhydride (polystyrene standards).

<sup>c</sup>G = glassy, S<sub>C</sub> = smectic C, I = isotropic. <sup>d</sup>DSC second heating scan under nitrogen (10 °C min<sup>-1</sup>). <sup>e</sup>DSC first cooling scan under nitrogen (-10 °C min<sup>-1</sup>). <sup>f</sup>Enthalpy of the transition between the smectic and isotropic phases. <sup>g</sup>The temperatures at 5% weight loss of the polymers under nitrogen determined by TGA heating experiments (10 °C min<sup>-1</sup>).

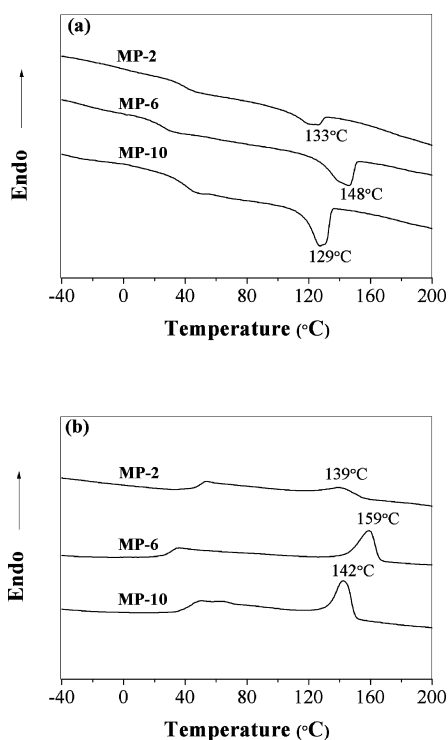


**Figure 2.** DSC curves of the main-chain azo polymers from the first cooling scan (a) and from the second heating scan (b) ( $\pm 10$  °C min<sup>-1</sup>).

main-chain azo polymers (Figure 3) and the phase transition peaks in the DSC curves of these azo polymers represented the transition between liquid crystalline and isotropic phases. The clearing temperatures ( $T_{cl}$ ) determined from the DSC second heating scan were 139, 159, and 142 °C for MP-2, MP-6, and MP-10, respectively (Table 1). The above results demonstrate that all the obtained main-chain azo polymers have a relatively broad range of liquid crystalline mesophases and low  $T_g$  values. It is worth mentioning here that the influence of the flexible spacer length has been reported for main-chain LCPs with rod-like mesogens and the transition temperatures ( $T_g$  or  $T_{cl}$ ) usually have a tendency to decrease with increasing the spacer

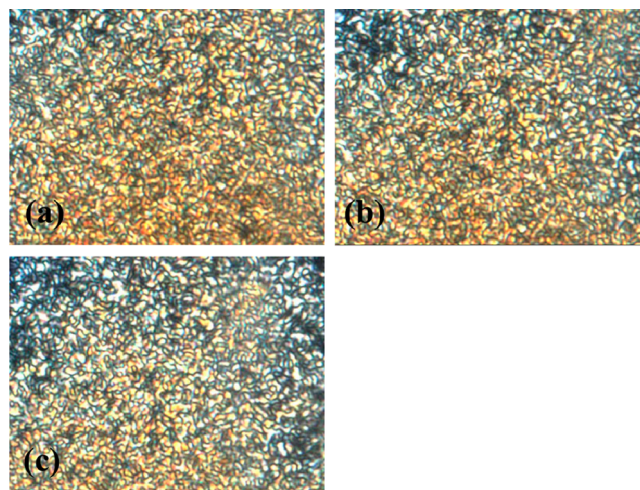


**Figure 3.** POM images upon cooling: MP-2 at 118 °C (annealed for 30 min) (a), MP-6 at 144 °C (annealed for 30 min) (b), and MP-10 at 124 °C (annealed for 30 min) (c).

length (with an evident even-odd effect).<sup>39-41</sup> However, no regular changes with spacer length were observed for our main-chain azo polymers, just as reported by Xu and co-workers.<sup>42</sup> The real reason is not very clear yet, and further investigation is ongoing to provide a reasonable explanation for this phenomenon.

It is well-known that SAXS can provide useful information concerning molecular arrangement, packing mode of the mesogen, and type of order in the mesophase of a liquid crystalline polymer, and it has thus been widely utilized for accurately assigning the exact nature of the liquid crystalline phases.<sup>26,43,44</sup> Therefore, the liquid crystalline mesophases of the main-chain azo polymers MP- $m$  ( $m = 2, 6, 10$ ) were further studied with *in situ* variable temperature SAXS. Figure 4a shows the SAXS patterns of MP-2, MP-6, and MP-10, which were

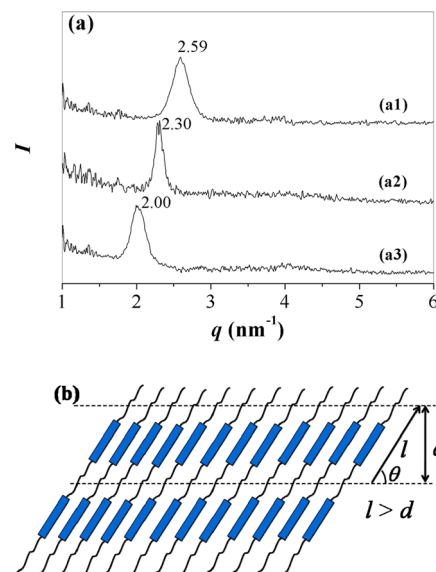


**Figure 4.** (a) SAXS patterns of the main-chain azo polymers upon cooling from the isotropic states: MP-2 at 118 °C (scan time: 20 min) (a1), MP-6 at 144 °C (scan time: 20 min) (a2), and MP-10 at 124 °C (scan time: 20 min) (a3). (b) Proposed liquid crystalline structure for MP- $m$  ( $m = 2, 6, 10$ ).

obtained at their liquid crystalline temperatures (with a certain time of annealing) upon cooling from the isotropic states. It can be seen clearly that each polymer exhibited one strong scattering peak at the small angle area, suggesting the existence of an ordered smectic lamellar structure with a layer spacing  $d$  ( $d = 2\pi/q$ , Table 2).<sup>44</sup> This  $d$  value is smaller than the

**Table 2. SAXS Characterization Data of the Azo Main-Chain LCPs**

sample	$q_1^a$ ( $\text{nm}^{-1}$ )	$d^b$ (nm)	$l^c$ (nm)	$d/l$	$\theta^d$ (deg)	liquid crystalline mesophase <sup>e</sup>
MP-2	2.59	2.43	2.79	0.87	60	S <sub>C</sub>
MP-6	2.30	2.73	3.19	0.86	60	S <sub>C</sub>
MP-10	2.00	3.14	3.59	0.87	60	S <sub>C</sub>

<sup>a</sup> $q_1$  refers to the scattering vector of the first-order diffraction peak of the azo polymers, as shown in Figure 4a. <sup>b</sup> $d$  denotes the layer spacing of the ordered smectic lamellar structures in the studied azo polymers determined by SAXS, which can be evaluated by using the equation  $d = 2\pi/q_1$ . <sup>c</sup> $l$  refers to the calculated molecular length for the fully extended liquid crystalline unit in the azo polymers. <sup>d</sup> $\theta$  represents the angle between the director of the azo mesogen and the smectic lamellar layer surface in the liquid crystalline states of the azo polymers, as shown in Figure 4b and  $\sin \theta = d/l$ . <sup>e</sup>S<sub>C</sub> refers to smectic C liquid crystalline mesophase.

calculated molecular length ( $l$ ) for the fully extended liquid crystalline unit, suggesting a smectic C structure with a tilted angle of 60° between the director of the azo mesogen and the smectic lamellar layer surface, as schematically shown in Figure 4b. This result agrees well with the schlieren textures observed (with POM) for the main-chain azo polymers and the general rule “schlieren texture is frequently found in the smectic C phase instead of smectic A phase”.<sup>45</sup>

**Chemical Reactivity of the Azo Main-Chain LCPs.** It is anticipated that the presence of the secondary amino groups in MP- $m$  ( $m = 2, 6, 10$ ) should make these azo polymers reactive precursors for further cross-linking and functionalization. Herein, we started to study the chemical cross-linking of the main-chain azo LCPs by using 1,6-hexamethylene diisocyanate (HDI) as the model cross-linker. The representative reactive azo main-chain LCP MP-6 was found to be able to directly react with HDI to provide the cross-linked main-chain azo polymers. Obvious gelating phenomenon was observed after the addition of HDI into the polymer solutions, suggesting the occurrence of the cross-linking reaction. Cross-linked polymers (namely CL-MP-6- $f$  ( $f = 2, 4$ )) were obtained by reacting MP-6 with varying amounts of HDI, where CL-MP-6 denotes the cross-linked polymer of MP-6 and  $f$  represents the molar ratio of the repeat unit (or reactive secondary amino group) in the polymer to HDI, respectively. The DSC study showed that no phase transition peak was discernible for the obtained cross-linked polymers in the studied temperature range (Figure S2). This, together with their presence of obvious optical birefringence in both the heating and cooling processes (as observed by POM) (Figure S3e,f), revealed that all these cross-linked main-chain azo polymers exhibited rather stable liquid crystalline phases. However, such cross-linked liquid crystalline phases proved to be rather difficult to develop, even after a long annealing time, probably due to the possible confinement effect of the cross-linking on the movement of the mesogens.<sup>26</sup>

The high chemical reactivity of the above-obtained azo main-chain LCPs was further demonstrated by reacting MP-6 with some anhydrides including acetic anhydride, Boc anhydride,

and methacrylic anhydride at ambient temperature (Scheme S1). A series of new functionalized main-chain azo polymers (i.e., A-MP-6, B-MP-6, and M-MP-6) were readily synthesized in high yields, with all of them showing obvious liquid crystalline phases (Figures S2 and S3b–d). Figure 1d–f presents the <sup>1</sup>H NMR spectra of these anhydride-modified MP-6.

**Photoresponsive Behaviors of the Azo Main-Chain LCPs and Their Supramolecular Hydrogen-Bonded Fibers.** The photoresponsive properties of the representative azo main-chain LCP MP-6 were first investigated in chloroform. By irradiation at 365 nm, the studied polymer solution underwent *trans* to *cis* photoisomerization until a photostationary state was eventually reached (Figure 5a). The intensity

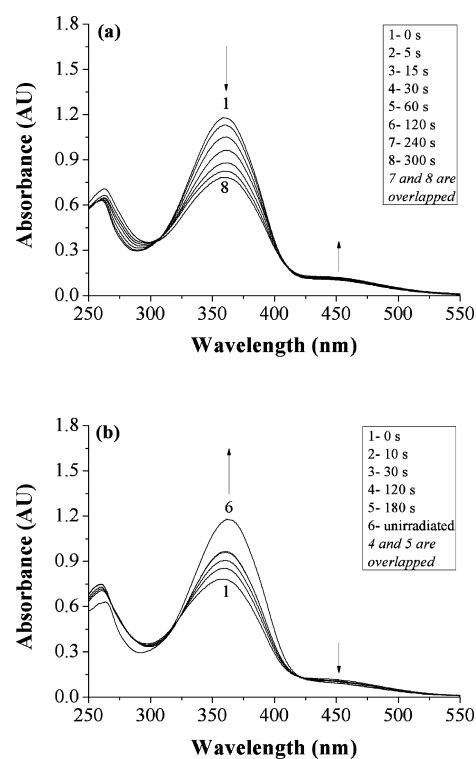


**Figure 5.** UV–vis spectral changes in dependence of time for the solution of MP-6 in chloroform ( $C = 50 \mu\text{M}$  repeat unit of the studied polymer) at 25 °C upon irradiation with 365 nm UV light (a) and upon irradiating the polymer solution at the photostationary state with visible light ( $\lambda > 430 \text{ nm}$ ) (b).

of the  $\pi \rightarrow \pi^*$  transition band around 360 nm decreased, whereas that of the  $n \rightarrow \pi^*$  transition band around 450 nm slightly increased. The existence of isobestic points at 304 and 410 nm is characteristic for the presence of two distinct absorbing species in equilibrium with each other and at the same time proves that no side reaction took place during the photoisomerization process in the range studied.<sup>46</sup> Irradiation of the above polymer solution at the photostationary state with visible light ( $\lambda > 430 \text{ nm}$ ) led to the *cis* to *trans* back-isomerization process (Figure 5b). However, the finally recovered absorbance of *trans*-isomer was lower than that before UV irradiation with the recovery of the *trans*-isomer being around 87%, just as previously reported by our group<sup>26,36,43</sup> and by others.<sup>47,48</sup> Its real cause is not totally clear yet but might be that, at the same wavelength where *cis* to *trans* photochemical back-isomerization was performed, there

was also a weak absorption from the *trans*-isomer, which eventually led to an equilibrium with *cis* to *trans* and *trans* to *cis* isomerizations taking place under the same visible light after most of the *cis*-isomer returned to the *trans*-isomer.<sup>26,49</sup> Nevertheless, the photoisomerization became completely reversible upon the subsequent cycles of UV and visible light irradiation (Figure S4).

The photoresponsive behaviors of the polymer fibers of MP-*m* (*m* = 2, 6, 10) were then studied. The fibers of these azo main-chain LCPs were fabricated by using the simple melt spinning method as reported previously,<sup>23,38</sup> but in the absence of any chemical cross-linker. POM (with crossed polarizer and analyzer) observation demonstrated that the obtained main-chain LCP fibers had a rather high order of mesogen along the fiber axis, as revealed by the sharp contrast inversion every 45° upon rotating the sample with respect to the analyzer (Figure 6a and Figure S5).<sup>23,38</sup> In addition, it can be envisioned that

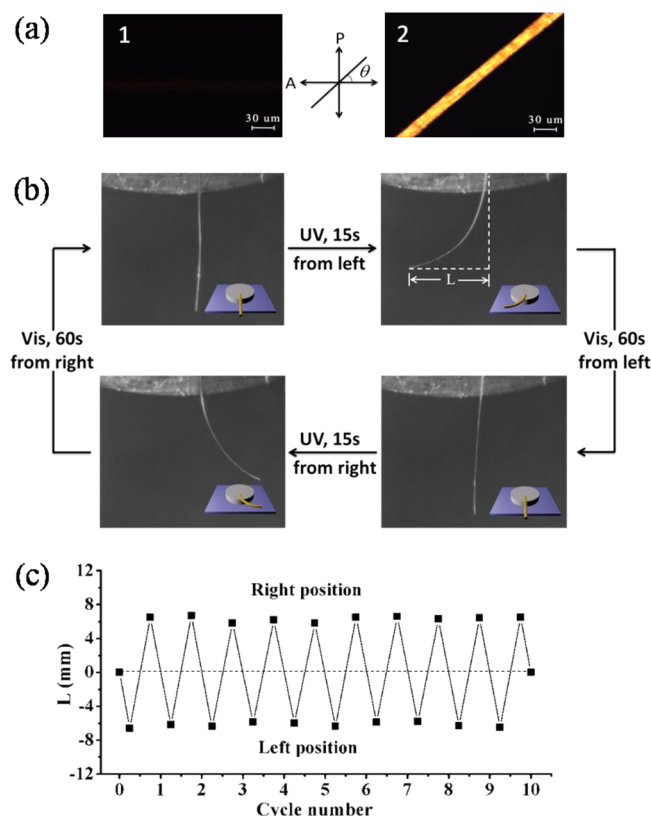


**Figure 6.** (a) POM images of the textures of the MP-6 fiber taken at room temperature. Sample angle to the analyzer:  $\theta = 0^\circ$  (1);  $\theta = 45^\circ$  (2). (b) Photographs of the MP-6 fiber that exhibit photoinduced bending and unbending behaviors upon irradiation with 365 nm UV light ( $150 \text{ mW cm}^{-2}$ ) and visible light ( $\lambda > 430 \text{ nm}$ ,  $120 \text{ mW cm}^{-2}$ ) at  $60^\circ\text{C}$ . (c) The reversible deformation of the MP-6 fiber characterized by tracing the bent distance from its straight state at  $60^\circ\text{C}$ . The size of the fiber is  $11 \text{ mm} \times 21 \mu\text{m}$ .

hydrogen bonding interactions should be present among the main-chain azo polymer chains because of their presence of the secondary amino groups, thus leading to supramolecular hydrogen bonding-cross-linked fibers.

To confirm the presence of hydrogen bonding interactions among the azo main-chain LCP chains, the variable temperature FT-IR experiments were performed for the representative polymer MP-6. Figure 7 shows the variable temperature FT-IR

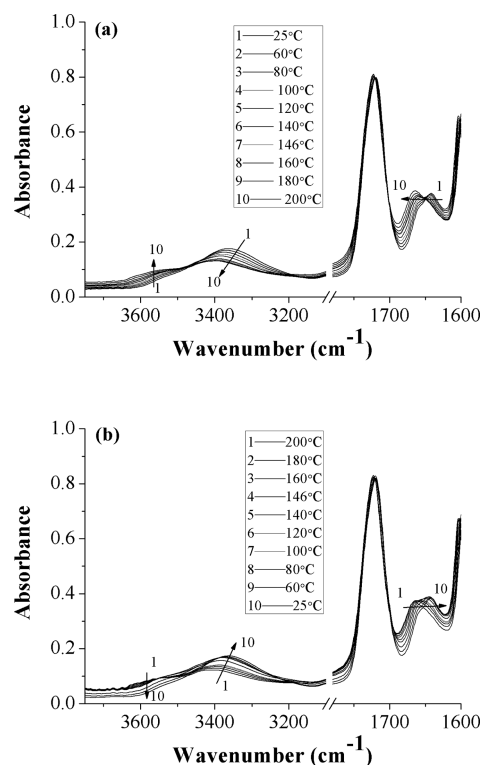


**Figure 7.** FT-IR spectra of MP-6 at different temperatures during the second heating (a) and first cooling (b) processes.

spectra of MP-6 obtained during both the second heating and first cooling processes. It can be seen clearly that MP-6 exhibits two infrared bands around  $3550 \text{ cm}^{-1}$  (very weak shoulder) and  $3360 \text{ cm}^{-1}$  (medium peak) for  $\nu_{\text{N-H}}$  at ambient temperature, which can be assigned to the “free” (higher than  $3400 \text{ cm}^{-1}$ ) and hydrogen-bonded N–H stretching modes, respectively. Moreover, the N–H stretching vibration also proved to be dependent on the sample’s temperature. The hydrogen-bonded N–H stretching peak (with a frequency lower than  $3400 \text{ cm}^{-1}$ ) became weaker and shifted toward higher frequencies upon increasing the sample temperature, while the free N–H stretching peak with a frequency higher than  $3400 \text{ cm}^{-1}$  became stronger in the meantime (Figure 7a), indicating that the hydrogen bonding in the polymer got weaker and some of the hydrogen-bonded N–H groups were transformed to free ones with increasing temperature (note that the hydrogen bonding still existed in the polymer even at  $200^\circ\text{C}$ ). On the other hand, the intensity and frequency of the N–H stretching vibration were fully recovered upon decreasing the sample temperature, suggesting that the hydrogen bonding interaction was reversible, just as expected (Figure 7b). It is noteworthy that the N–H bending vibration band of the studied polymer also showed an obvious reversible change in its frequency (from  $1641$  to  $1665 \text{ cm}^{-1}$ )<sup>50</sup> following the change of the sample temperatures, whereas negligible frequency shift (from  $1719$  to  $1723 \text{ cm}^{-1}$ ) was observed for the C=O stretching band from the ester groups in the polymer, which clearly demonstrated that the hydrogen bonding mainly formed between N–H and N–H (both from the secondary amino groups) instead of between the N–H and C=O (from the ester groups in the polymer).

With the above-obtained supramolecular hydrogen-bonded polymer fibers in hand, we started to study their photo-

mechanical properties. Part of MP-6 fiber was first pasted onto an aluminum block and heated to 60 °C by a hot stage (Figure S6a). Figure 6b shows the photoinduced bending and unbending of the MP-6 fiber upon irradiation with UV light and visible light, respectively. It can be seen clearly that the MP-6 fiber bent to the left side toward the actinic light source along the fiber axis when it was exposed to 365 nm UV light (150 mW cm<sup>-2</sup>) from the left side of the sample, and it took a bending time of 15 s for the fiber to reach its maximum bending. The bent fiber could revert to its initial straight state upon irradiation with visible light ( $\lambda > 430$  nm, 120 mW cm<sup>-2</sup>) for 60 s. In addition, upon subsequent irradiation with the same UV and visible light from the right side, the MP-6 fiber also bent to the right side toward the actinic light source and then reverted to its initial straight state, respectively. The above results unambiguously demonstrated that the bending and unbending of the fiber were fast and reversible and could be easily controlled by just changing the wavelength of the incident light. In addition, the bending direction of the fiber could be directly controlled by changing the irradiation direction of the light, thus allowing the well-controlled three-dimensional photomobility of the fiber on demand. Similar with the MP-6 fiber, MP-2 and MP-10 fibers also showed fast and reversible photoinduced bending and unbending under the similar conditions (Figure S6b,c). These reversible photoinduced bending and unbending of the physically cross-linked azo main-chain LCP fibers are quite similar to those of the previously reported chemically cross-linked azo LCP fibers and can also be explained by the same mechanism.<sup>23</sup> However, in comparison with the chemically cross-linked azo LCPs normally used for the photomechanical studies, this physically cross-linked photomechanical system has some distinct advantages such as greater flexibility in fabrication and more freedom for further processing.<sup>51–53</sup> Although a few photo-deformable LCPs with physically cross-linked networks have been disclosed, they are all based on the LCPs with azo moieties in the side chains.<sup>22,52,53</sup> *To our knowledge, our findings presented here is the first successful example of the physically cross-linked photomechanical system based on the main-chain LCPs with azo units in the polymer backbones.*

The reversible deformation of the azo main-chain LCP fibers upon irradiation with UV light and visible light was also studied, which was found to be capable of being repeated over 100 cycles, and both their bending/unbending times and bending angles remained almost constant, thus demonstrating the excellent fatigue resistance of these photodeformable supramolecular hydrogen-bonded LCP fibers.<sup>54</sup> Figure 6c shows the initial 10 cycles of the reversible deformation of the MP-6 fiber. Note that the oriented fibers of the main-chain azo polymers obtained by the reaction of the secondary amino groups of MP-6 with anhydrides were also prepared via the melt spinning method, but they could not show any photoinduced bending behavior, thus revealing that the presence of hydrogen bonding interactions between the polymer chains is necessary for achieving the photomechanical properties of such fibers.

In addition to the above reversible photoinduced bending and unbending of the polymer fibers upon irradiation with UV light and visible light, we also studied the UV-induced bending and thermally induced unbending behaviors of the MP-6 fiber. It is expected that an unbending process should take place for the UV light-deformed polymer fiber when the UV light irradiation was turned off because of the occurrence of the *cis* to

*trans* thermal back-isomerization of the azo groups in the fiber. This hypothesis was indeed verified by the experimental results (Figure S7a). The UV light-induced bending and thermally induced unbending proved to be reversible although the thermally induced unbending took a relatively longer time (140 s) for the fiber to revert to its initial straight state in comparison with the visible light-induced unbending process (60 s). Moreover, such bending and unbending could also be repeated over 100 cycles, and both their bending/unbending times and bending angles remained almost constant, again demonstrating the excellent fatigue resistance of the fiber. Figure S7b shows the initial 10 cycles of the reversible deformation of the MP-6 fiber.

The dependence of the bending behaviors of the supramolecular hydrogen-bonded fibers on the light intensity and temperature was studied by measuring the bending times for the fibers to bend to their largest extent (which proved to be almost independent of the light intensity and temperature ( $T > T_g$ )) upon exposure to 365 nm UV light (Figure 8). The

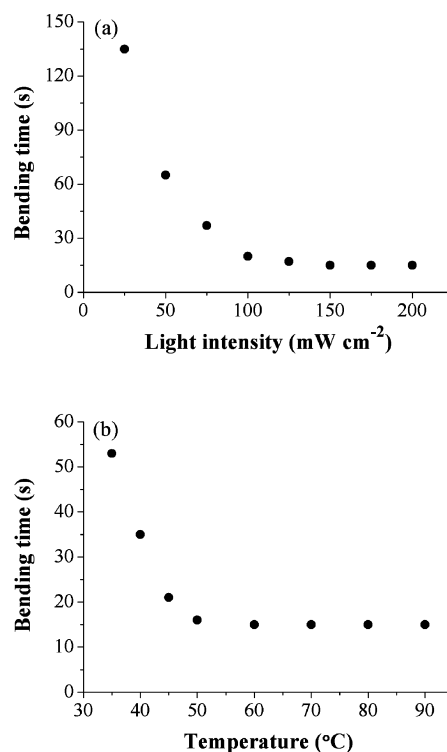


**Figure 8.** (a) Effect of light intensity on the bending time (i.e., the time required to reach the maximum bending) of the MP-6 fiber upon its exposure to 365 nm UV light at 60 °C. (b) Effect of temperature on the bending time of the MP-6 fiber upon its exposure to 365 nm UV light (150 mW cm<sup>-2</sup>). The size of the fiber is 11 mm × 21 μm.

experimental results revealed that the photoinduced bending could take place only when the fibers were heated to a temperature above the  $T_g$  of MP-*m* ( $m = 2, 6, 10$ ), which is easily understandable because the relaxation of polymer segments is necessary to transfer the changes in structure and alignment of the azo moieties at the fiber surface to the transformation of the conformation in the entire physically cross-linked network, just as in the chemically cross-linked azo LCP systems.<sup>55</sup> Figure 8 shows that a rapid decrease in the bending time was observed for the MP-6 fiber both with an increase in the 365 nm UV light intensity from 25 to 100 mW

$\text{cm}^{-2}$  at 60 °C and with an increase in the temperature from 35 to 50 °C under the 365 nm UV light irradiation with a fixed intensity ( $150 \text{ mW cm}^{-2}$ ). However, the bending time remained almost unchanged with a further increase in the light intensity and temperature. Similar results were also reported and explained previously by Yu et al.<sup>55</sup> Note that the photoinduced bending of the MP-6 fiber could be realized even at close to ambient temperature (i.e., 35 °C) within 1 min (Figure 8b), mainly because of the low  $T_g$  of MP-6. The MP-2 and MP-10 fibers also showed similar dependence of the bending behaviors on the light intensity and temperature as the MP-6 fiber (Figures S8 and S9).

The mechanical properties and photoinduced mechanical force (or stress) of the photodeformable azo main-chain LCP fibers were also investigated because they are important parameters for the potential applications of such fibers in artificial muscles and light-driven actuators. Figure 9a presents

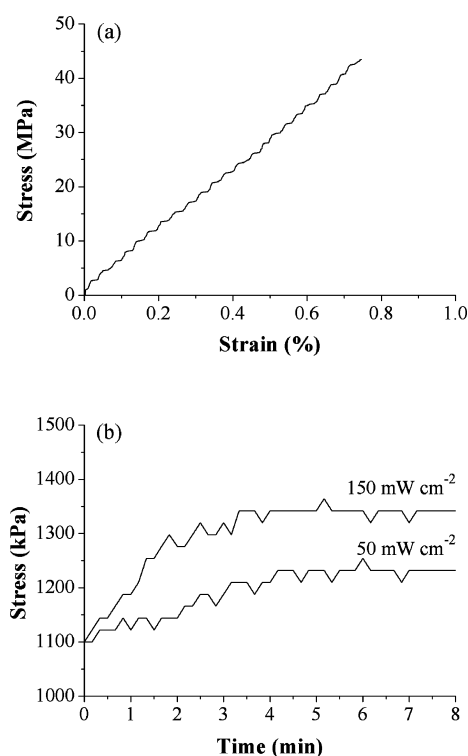


**Figure 9.** (a) Stress–strain curve of the MP-6 fiber (size:  $10 \text{ mm} \times 25 \mu\text{m}$ ) measured at 28 °C. (b) Change in the stress of the MP-6 fiber (size:  $9 \text{ mm} \times 24 \mu\text{m}$ ) upon its exposure to 365 nm UV light with different light intensities at 35 °C. An external stress of 1100 kPa was loaded initially on the fiber to keep its length constant.

the stress–strain curve of the MP-6 fiber determined by thermomechanical analysis (TMA) at 28 °C. The polymer fiber achieves a tensile strength of 44 MPa and an elastic moduli of 5.8 GPa (i.e., elastic moduli = stress/strain), which is about 2.8 and 14.5 times as large as the tensile strength (i.e., 16 MPa) and elastic moduli (i.e., 400 MPa) of a chemically cross-linked azo LCP film, respectively,<sup>54</sup> thus demonstrating the good mechanical properties of our supramolecular hydrogen-bonded main-chain LCP fibers. The mechanical stress generated in the MP-6 fiber upon photoirradiation was also measured by TMA. One fiber with a length of 9 mm and a diameter of  $24 \mu\text{m}$  was fixed by clamping its two ends and then heated to 35 °C, which is 5 °C higher than the  $T_g$  of MP-6. An initial stress of 1100 kPa

was loaded onto the fiber to keep its length constant. The stretching direction was controlled to be parallel to the fiber axis. Figure 9b shows the change in the stress of the fiber upon its exposure to 365 nm UV light with different intensities at 35 °C. A clear increase in the stress was observed for the fiber, indicating the generation of the mechanical force in the fiber under photoirradiation. The generated maximum stress was determined to be 130 and 240 kPa when the light intensity was 50 and  $150 \text{ mW cm}^{-2}$ , respectively, which are close to the stress generated by the chemically cross-linked azo LCP films<sup>56</sup> and fibers<sup>23</sup> as well as that of the human muscles (around 300 kPa).<sup>23,56</sup> The higher intensity of UV light generated larger stress, which could be ascribed to the higher concentration of *cis*-azo moieties produced by the actinic light with a higher intensity and thus the larger surface contraction.

## CONCLUSIONS

We have demonstrated for the first time the efficient synthesis of a series of azo main-chain LCPs with reactive secondary amino groups in the polymer backbones via the facile Michael addition polymerization under mild reaction conditions. These main-chain azo polymers showed rather high thermal stability, relatively low glass transition temperatures, a broad temperature range of smectic C liquid crystalline mesophases, and reversible photochemical behaviors. In addition, they proved to be highly reactive precursors for various advanced functional linear and cross-linked azo main-chain LCPs. Furthermore, these azo main-chain LCPs could be directly used to fabricate supramolecular hydrogen-bonded LCP fibers by the simple melt spinning method, which showed a high order of mesogen along the fiber axis and exhibited fast and reversible photoinduced bending and unbending behaviors with controllable three-dimensional photomobile directions upon their exposure to UV and visible light even at close to ambient temperature. In particular, the as-prepared supramolecular photomechanical system showed very good photodeformation fatigue resistance. The stress generated by one fiber under the UV light irradiation at 35 °C reached 240 kPa, which is similar to the contraction forces of both the chemically cross-linked photomechanical system and human muscles (around 300 kPa). Considering its highly appealing properties such as flexible preparation, high reconstruction and recycle ability, and good mechanical and photomechanical properties, we believe that such supramolecular hydrogen-bonded photomechanical system hold great promise in many potential applications such as artificial muscles and actuators.

## ASSOCIATED CONTENT

### Supporting Information

Scheme for the polymer analogous reactions of MP-6 with a series of anhydrides, dependence of the yields of MP-6 on the polymerization time, DSC curves and POM images of the anhydride-modified linear polymers and HDI-cross-linked polymers of MP-6, UV and visible light-induced photoisomerization cycles of the MP-6 solution, POM images of the textures of the MP-2 and MP-10 fibers, photographs of the photoinduced bending and unbending of the MP-2 and MP-10 fibers as well as those of the UV-induced bending and thermally induced unbending of the MP-6 fiber, and the effects of light intensity and temperature on the bending times of the MP-2 and MP-10 fibers. This material is available free of charge via the Internet at <http://pubs.acs.org>.

## AUTHOR INFORMATION

## Corresponding Author

\*E-mail zhanghuiqi@nankai.edu.cn; Tel +86-22-23507193 (H.Z.).

## Notes

The authors declare no competing financial interest.

## ACKNOWLEDGMENTS

The authors gratefully acknowledge the financial support from National Natural Science Foundation of China (20974048, 51103075), Natural Science Foundation of Tianjin (10JCYBJC02100, 11JCYBJC01500), and PCSIRT (IRT1257).

## REFERENCES

- (1) Zhang, H.; Li, C.; Huang, W.; He, B. *Chin. Polym. Bull.* **1998**, *2*, 63–69.
- (2) Natansohn, A.; Rochon, P. *Chem. Rev.* **2002**, *102*, 4139–4175.
- (3) Shibaev, V.; Bobrovsky, A.; Boiko, N. *Prog. Polym. Sci.* **2003**, *28*, 729–836.
- (4) Ikeda, T. *J. Mater. Chem.* **2003**, *13*, 2037–2057.
- (5) Yu, Y.; Nakano, M.; Ikeda, T. *Nature* **2003**, *425*, 145.
- (6) Zhao, Y. *Pure Appl. Chem.* **2004**, *76*, 1499–1508.
- (7) Xie, P.; Zhang, R. *J. Mater. Chem.* **2005**, *15*, 2529–2550.
- (8) Li, M. H.; Keller, P. *Philos. Trans. R. Soc. London, Ser. A* **2006**, *364*, 2763–2777.
- (9) Ikeda, T.; Mamiya, J.; Yu, Y. *Angew. Chem., Int. Ed.* **2007**, *46*, 506–528.
- (10) Koerner, H.; White, T. J.; Tabiryan, N. V.; Bunning, T. J.; Vaia, R. A. *Mater. Today* **2008**, *11*, 34–42.
- (11) Van Oosten, C. L.; Bastiaansen, C. W. M.; Broer, D. J. *Nat. Mater.* **2009**, *8*, 677–682.
- (12) Ohm, C.; Brehmer, M.; Zentel, R. *Adv. Mater.* **2010**, *22*, 3366–3387.
- (13) Schumers, J. M.; Fustin, C. A.; Gohy, J. F. *Macromol. Rapid Commun.* **2010**, *31*, 1588–1607.
- (14) Yu, H.; Ikeda, T. *Adv. Mater.* **2011**, *23*, 2149–2180.
- (15) Yang, H.; Ye, G.; Wang, X.; Keller, P. *Soft Matter* **2011**, *7*, 815–823.
- (16) Broer, D. J.; Bastiaansen, C. M. W.; Debije, M. G.; Schenning, A. P. H. J. *Angew. Chem., Int. Ed.* **2012**, *51*, 7102–7109.
- (17) Wang, W.; Sun, X.; Wu, W.; Peng, H.; Yu, Y. *Angew. Chem., Int. Ed.* **2012**, *51*, 4644–4647.
- (18) Zettsu, N.; Ubukata, T.; Seki, T.; Ichimura, K. *Adv. Mater.* **2001**, *13*, 1693–1697.
- (19) Takase, H.; Natansohn, A.; Rochon, P. *Polymer* **2003**, *44*, 7345–7351.
- (20) Zettsu, N.; Seki, T. *Macromolecules* **2004**, *37*, 8692–8698.
- (21) Finkelmann, H.; Nishikawa, E.; Pereira, G. G.; Warner, M. *Phys. Rev. Lett.* **2001**, *87*, 015501.
- (22) Mamiya, J.; Yoshitake, A.; Kondo, M.; Yu, Y.; Ikeda, T. *J. Mater. Chem.* **2008**, *18*, 63–65.
- (23) Yoshino, T.; Kondo, M.; Mamiya, J.; Kinoshita, M.; Yu, Y.; Ikeda, T. *Adv. Mater.* **2010**, *22*, 1361–1363.
- (24) Zettsu, N.; Ogasawara, T.; Arakawa, R.; Nagano, S.; Ubukata, T.; Seki, T. *Macromolecules* **2007**, *40*, 4607–4613.
- (25) Gu, H. W.; Xie, P.; Shen, D. Y.; Fu, P. F.; Zhang, J. M.; Shen, Z. R.; Tang, Y. X.; Cui, L.; Kong, B.; Wei, X. F.; Wu, Q.; Bai, F. L.; Zhang, R. B. *Adv. Mater.* **2003**, *15*, 1355–1358.
- (26) Li, X.; Wen, R.; Zhang, Y.; Zhu, L.; Zhang, B.; Zhang, H. *J. Mater. Chem.* **2009**, *19*, 236–245.
- (27) Acierno, D.; Amendola, E.; Bugatti, V.; Concilio, S.; Giorgini, L.; Iannelli, P.; Piotta, S. P. *Macromolecules* **2004**, *37*, 6418–6423.
- (28) Xue, X.; Zhu, J.; Zhang, Z.; Zhou, N.; Tu, Y.; Zhu, X. *Macromolecules* **2010**, *43*, 2704–2712.
- (29) Irie, M.; Hirano, Y.; Hashimoto, S.; Hayashi, K. *Macromolecules* **1981**, *14*, 262–267.
- (30) Irie, M.; Schnabel, W. *Macromolecules* **1981**, *14*, 1246–1249.
- (31) Xu, C.; Wu, B.; Becker, M. W.; Dalton, L. R.; Ranon, P. M.; Shi, Y.; Steier, W. H. *Chem. Mater.* **1993**, *5*, 1439–1444.
- (32) Yu, X.; Luo, Y.; Deng, Y.; Yan, Q.; Zou, G.; Zhang, Q. *Eur. Polym. J.* **2008**, *44*, 881–888.
- (33) Hosono, N.; Yoshikawa, M.; Furukawa, H.; Totani, K.; Yamada, K.; Watanabe, T.; Horie, K. *Macromolecules* **2013**, *46*, 1017–1026.
- (34) Mather, B. D.; Viswanathan, K.; Miller, K. M.; Long, T. E. *Prog. Polym. Sci.* **2006**, *31*, 487–531.
- (35) Zhang, H.; Huang, W.; Li, C.; He, B. *Acta Polym. Sin.* **1999**, *1*, 48–54.
- (36) Li, X.; Fang, L.; Hou, L.; Zhu, L.; Zhang, Y.; Zhang, B.; Zhang, H. *Soft Matter* **2012**, *8*, 5532–5542.
- (37) Kane, B. E.; Grant, M. K.; El-Fakahany, E. E.; Ferguson, D. M. *Bioorg. Med. Chem.* **2008**, *16*, 1376–1392.
- (38) Naciri, J.; Srinivasan, A.; Jeon, H.; Nikolov, N.; Keller, P.; Ratna, B. R. *Macromolecules* **2003**, *36*, 8499–8505.
- (39) Antoun, S.; Lenz, R. W.; Jim, J. I. *J. Polym. Sci., Polym. Chem. Ed.* **1981**, *19*, 1901–1920.
- (40) Kantor, S. W.; Sung, T. C.; Atkins, E. D. T. *Macromolecules* **1992**, *25*, 2789–2795.
- (41) Kantor, S. W.; Sung, T. C. *Macromolecules* **1993**, *26*, 3758–3763.
- (42) Wu, W.; Li, Z.; Zhou, Q. F.; Ye, M.; Xu, M. *Chin. J. Polym. Sci.* **1994**, *12*, 337–344.
- (43) Li, Z.; Zhang, Y.; Zhu, L.; Shen, T.; Zhang, H. *Polym. Chem.* **2010**, *1*, 1501–1511.
- (44) Chen, X. F.; Tenneti, K. K.; Li, C. Y.; Bai, Y.; Wan, X.; Fan, X. H.; Zhou, Q. F.; Rong, L.; Hsiao, B. S. *Macromolecules* **2007**, *40*, 840–848.
- (45) Cheng, Y. H.; Chen, W. P.; Shen, Z.; Fan, X. H.; Zhu, M. F.; Zhou, Q. F. *Macromolecules* **2011**, *44*, 1429–1437.
- (46) Niemann, M.; Ritter, H. *Makromol. Chem.* **1993**, *194*, 1169–1181.
- (47) Wang, G.; Tong, X.; Zhao, Y. *Macromolecules* **2004**, *37*, 8911–8917.
- (48) Akiyama, H.; Tamaoki, N. *Macromolecules* **2007**, *40*, 5129–5132.
- (49) Li, M. H.; Keller, P.; Li, B.; Wang, X.; Brunet, M. *Adv. Mater.* **2003**, *15*, 569–572.
- (50) Silverstein, R. M.; Webster, F. X.; Kiemle, D. J. *Spectrometric Identification of Organic Compounds*; John Wiley & Sons: Hoboken, NJ, **2005**.
- (51) Ahir, S. V.; Tajbakhsh, A. R.; Terentjev, E. M. *Adv. Funct. Mater.* **2006**, *16*, 556–560.
- (52) Choi, H. J.; Jeong, K.-U.; Chien, L.-C.; Lee, M.-H. *J. Mater. Chem.* **2009**, *19*, 7124–7129.
- (53) Kim, D.-Y.; Lee, S.-A.; Choi, H. J.; Chien, L.-C.; Lee, M.-H.; Jeong, K.-U. *J. Mater. Chem. C* **2013**, *1*, 1375–1382.
- (54) Sun, X.; Wang, W.; Qiu, L.; Guo, W.; Yu, Y.; Peng, H. *Angew. Chem., Int. Ed.* **2012**, *51*, 8520–8524.
- (55) Yu, Y.; Nakano, M.; Ikeda, T. *Pure Appl. Chem.* **2004**, *76*, 1467–1477.
- (56) Yu, Y.; Maeda, T.; Mamiya, J.; Ikeda, T. *Angew. Chem., Int. Ed.* **2007**, *46*, 881–883.